# 9,10-Dihydroanthracene auto-photooxidation efficiently triggered photocatalytic oxidation of organic compounds by molecular oxygen under visible light

Dabo Jiang, Mengke Chen, Youer Deng, Wenwei Hu, Anqun Su, Bo Yang, Feng Mao, Chao Zhang, Yachun Liu, Zaihui Fu*

*National and Local Joint Engineering Laboratory for New Petro-chemical Materials and Fine Utilization of Resources and Key Laboratory of Chemical Biology and Traditional Chinese Medicine Research (Ministry of Education of China), College of Chemistry and Chemical Engineering, Hunan Normal University, Changsha Hunan 410081, China*

## ARTICLE INFO

## ABSTRACT

The development of mild and efficient process for the selective oxidation of organic compounds by molecular oxygen ($O_2$) can be one of the key technologies for synthesizing oxygenates. This paper discloses an efficient and mild synthesis protocol for the $O_2$-involved ethylbenzene (EB) photooxidation triggered by 910-dihydroanthracene (DHA) auto- photooxidation in acetone under visible light illumination, which can achieve 87.7 % EB conversion and 99.5 % acetylacetone (ACP) selectivity under ambient conditions. Also, 62.9 % EB conversion and 96.3 % ACP selectivity is obtained in air atmosphere. Furthermore, this protocol has a good adaptability for the photooxidation of other organic substrates such as tetrahydronaphthalene, diphenylmethane, toluene, cyclohexane, cyclohexene, alcohol, methylfuran and thioether to their corresponding oxygenates. A series of control and quenching tests, combined with EPR spectra, suggest that the photo-excited DHA can transfer its photo-electron to $O_2$ to yield a superoxide radical anion ($O_2^{\bullet-}$), then DHA is preferentially oxidized to anthraquinone (AQ) by the active $O_2^{\bullet-}$ owing to its high reactivity. Finally, the in situ generated AQ as an active photo-catalyst can achieve the photooxidation of EB and other organic compounds by $O_2$. The present photo-autoxidation protocol gives a good example for the $O_2$-based selective oxidation of inert hydrocarbons under mild conditions.

## Introduction

The selective oxidation of hydrocarbons to the corresponding oxygen-containing compounds, including alcohols, aldehydes, ketones, epoxides, and carboxylic acids, is one of the most important and challenging reactions in the chemical industry [1,2]. Recently, the selective oxidation of ethylbenzene (EB) to the higher-value-added product acetophenone (ACP) has received increasing attention because ACP is used as an intermediate for the manufacture of some perfumes, pharmaceuticals, resins, alcohols, aldehydes and esters [3–5]. Traditionally, ACP is synthesized by Friedel-Crafts acylation of arenes by acyl halides or acid anhydrides with Lewis acids as catalysts [6] or by the oxidation of alkylarenes with stoichiometric inorganic oxidants, such as permanganate or dichromate [7]. Unfortunately, Friedel-Crafts acylation needs to use large amount of Lewis acid catalyst (at least 1.2 eq relative to the substrate), which drastically increases a burden of product

separation. Not only the stoichiometric oxidation needs to consume large quantities of oxidants but also produces large quantities of noxious and corrosive wastes, and separating reactants and products from the liquid reaction mixture are difficult. Recently, considerable research efforts have been dedicated to the selective oxidation of EB to ACP by using various heterogeneous catalysts including alumina/silica supported Mn-containing complexes [8–10], supported Co-containing complexes [11–15], Cr-, Mn-, Co- and Ce-containing mesoporous molecular sieves [16–20], as well as Mn- and Cu-containing hydrotalcites [4,21–23]. Table 1 lists some representative catalysis oxidation systems for the synthesis ACP from EB. In that, the use of tert-butyl hydroperoxide (TBHP) as an oxidant could usually obtain a high EB conversion (69–99 %) and ACP selectivity (80–99.9 %) at $80-120\,°C$ [24–27], but its excessive use results in a significant increase in cost. The molecular oxygen ($O_2$)-involved EB oxidation is highly appreciated owing to a low cost and an environmental friendliness, but this oxidation protocol

**Table 1**
Comparison of the results of oxidation reaction of EB under different oxidation systems.

| Entry | Catalyst | Oxidant/ (atm) | Solvent (mL) | T (°C) t (h) | EB Conv. (%) | ACP Sel. (%) | Ref. |
|---|---|---|---|---|---|---|---|
| 1 | A[a]-MMO | TBHP [b] | None | 120, 12 | 92.8 | 89.4 | [24] |
| 2 | N-GM-B [c] | TBHP [b] | H$_2$O (3) | 80, 24 | 97.5 | 97.2 | [25] |
| 3 | MMO-0.5/A [d] | TBHP [b] | None | 120, 12 | 69.5 | 80.4 | [26] |
| 4 | p-Co–N–C-700H [e] | TBHP [b] | H$_2$O (3) | 80, 12 | 99.8 | 99.9 | [27] |
| 5 | ZnCr-LDH/CNTs [f] | O$_2$ (10) | None | 130, 6 | 54.2 | 93.7 | [28] |
| 6 | CNTs–HCl [g] | O$_2$ (15) | MeCN (30) | 155, 4 | 35.6 | 61.1 | [29] |
| 7 | V$^{IV}$OQ$_2$/NHPI [h] | O$_2$ (1) | PhCN [i] (6) | 90, 12 | 69.0 | 97.0 | [30] |
| 8 | MPcTs-Zn$_2$Al-LDH/NHQI [j] | O$_2$ (1) | PhCN [i] (6) | 120, 24 | 90.0 | 99.0 | [31] |
| 9 [k] | TiO$_2$ | O$_2$ (1) | H$_2$O (13) | rt., 2 | 6.71 | 100 | [34] |
| 10 [l] | PW$_9$V$_3$-HCl | O$_2$ (1) | MeCN (5.5) | rt., 12 | 16.1 | 66.5 | [35] |
| 11 [l] | TMADT-HCl/H$_2$O | O$_2$ (1) | MeCN (5.5) | rt., 12 | 19.0 | 82.1 | [36] |
| 12 [l] | CQD/TBADT-HCl | O$_2$ (1) | MeCN (5) | rt., 12 | 20.4 | 78.7 | [37] |
| 13[m] | TCNS [n] | O$_2$ (1) | MeCN | 35, 6 | 58.0 | 55.2 | [38] |
| 14 [l] | DHA | O$_2$ (1) | Acetone (5) | rt., 12 | 87.7 | 99.5 | This work |
| 15 [l] | DHA | Air (1) | Acetone (5) | rt., 12 | 62.9 | 96.3 | This work |
| 16 [l] | AQ | O$_2$ (1) | Acetone (5) | rt., 12 | 86.5 | 99.8 | This work |

[a] A, Al$_2$O$_3$@CoCuAl; [b] TBHP, Tert-butyl hydroperoxide; [c] N-GM-B, N-doped graphene material (dealing with 1 M HCl); [d] Hierarchical flower-like core–shell structured Co-based mixed metal oxides; [e] Co and N co-doped carbon catalysts; [f] hybrid Zn–Cr layered double hydroxide/carbon nanotubes nanocomposite; [g] CNTs − HCl, CNTs were stirred in concentrated HCl for 6 h; [h] V$^{IV}$OQ$_2$, Oxobis (2,4-pentanedionate) vanadium (IV) (VIVO (acac)$_2$); [i] PhCN, benzonitrile; j Car-NHPI, 4-carboxylN-hydroxyphthalimide; NHQI, N-hydroxyquinolinimide; [k] 5 W UV–vis Pen Ray lamp; [l] Using 35 W tungsten–bromine lamp as visible-light source; [m] Solar light; [n] TiO$_2$ doped with C, N, and S elements.

usually needs to use a high temperature (130 − 155 °C) to efficiently activate the inert O$_2$, affording a relatively low efficiency (35–54 % EB conversion and 61–94 % ACP selectivity) [28,29]. N-hydroxyphthalimide (NHPI) combined V$^{IV}$OQ$_2$ [30], especially CoPcTs-Zn$_2$Al-LDHs [31], could efficiently catalyze the oxidation of EB by O$_2$ at 90 − 120 °C, giving a high EB conversion (69–95 %) and an excellent 90–99 % ACP selectivity. Unfortunately, the extensive use of expensive NHPI (about 10–20 %) and relatively harsh reaction conditions in this synthesis protocol elevate cost and energy consumption for the synthesis of ACP from EB. Photo-catalysis arises from synthetic, mechanistic, or environmental application that represents a key strategy for the development of sustainable methods for chemical transformations [32,33], and it has been successfully applied to the synthesis of ACP from EB oxidation with O$_2$ under very mild conditions. But the currently reported photo-catalysts such TiO$_2$ [34], PMoV − HCl [35], decatungstates (DTs) [36,37] have a much lower photooxidation efficiency than the above-mentioned thermal catalysis systems and the best catalyst TCNS [38] could only achieve 58 % EB conversion and 55 % ACP selectivity. It is, therefore, still an important and challenging task to develop a mild and highly efficient photo-synthetic protocol for the oxidation of EB to ACP by O$_2$, which can achieve almost equal efficiency to the highly efficient thermal catalysis oxidation systems.

Inspired by our recently reported work [39], visible light could directly trigger the oxidation of 910-dihydroanthracene (DHA) without any extra catalysts and additives under room temperature and 1 atm pure O$_2$ atmosphere, thereby quantitatively generating anthraquinone (AQ) as an active photo-catalyst, we suggest that the DHA-based autophtooxidation may be an efficient, eco-friendly and mild photo-synthetic protocol for converting relatively inert organic compounds to the corresponding oxygenated products. Herein, we would report the successful applications of this photo-synthetic protocol in the photooxidation of various organic compounds by O$_2$, which can meet the requirements of the green chemistry principles. In EB photooxidation, this protocol can achieve respectively 87.7 % EB conversion and 99.5 % ACP selectivity at room temperature under 12 h of visible light irradiation and pure O$_2$ atmosphere and even using air instead of pure O$_2$ can also achieve 62.9 % EB conversion and 96.3 % ACP selectivity, respectively, which has a remarkably comprehensive advantage over most of the oxidation systems in Table 1 previously reported. Furthermore, the DHA-based photo-synthetic protocol has a good adaptability for the selective oxidation of other organic substrates such as

tetrahydronaphthalene, diphenylmethane, cyclohexane, toluene (substituent toluene), methylfuran, cyclohexene, alcohol and thioether to their corresponding oxygenates, which gives a good example to propose a new method to the selective oxygenation of organic compounds by molecular oxygen.

## Experimental section

### Reagents and materials

Materials and reagents used in this study were 910-dihydroanthracene (DHA), cyclohexane, toluene, ethylbenzene, cyclohexanol, benzyl alcohol, diphenylmethane, tetrahydronaphthalene, cyclohexene, p-bromoethylbenzene, p-nitrotoluene, p-xylene, m-chlorotoluene, n-hexanol, n-pentane, 2-methylfuran, thioanisole, furfuryl alcohol, acetone, acetonitrile (MeCN), isopropanol (IPA), benzoquinone (BQ), anthraquinone (AQ), 2,2,6,6-Tetramethylpiperidinooxy (TEMPO), 5,5-Dimethyl-1-pyrroline N-oxide (DMPO), deuterated acetone (Acetone-d$_6$), N,N-dimethylformamide (DMF), N,N-dimethyl acetamide (DMA), all of which were of analytical grade.

### Characterization of samples

UV–vis spectra of the liquid samples in acetone were recorded from 200 to 800 nm on UV-2450 spectrophotometer (Shimadzu, Japan). Photo-luminescence (PL) spectra of the liquid samples in various solvents were carried out on fluorescence spectrophotometer (HITACHI F-7000) at room temperature. EPR spectra of the samples were measured in 50 μL quartz tubes on a Bruker A300 − 10/12/S at room temperature. The spectrometer at 9.8 GHz, modulation frequency 100 kHz, modulation amplitude 3 G. EPR spectra were simulated using an extended version of the program Bruker Win EPR.

### Visible-light-catalytic oxidation experiments

The visible light-driven oxygenation of ethylbenzene (EB) by O$_2$ in the presence of a catalytic amount of DHA was performed in a self-assembly common glass photo-reactor (Fig. S1) equipped with a water-cooled condenser and an oxygen storage vessel (1 atm) [40]. A 35 W tungsten–bromine lamp (purchased from NVC lighting corporation; Light intensity, 535 mW/cm$^2$; Operating voltage, 12 V; The emission

spectra of the tungsten–bromine lamp is shown in Fig. S2) came with an UV light filter (Osram brand) was immersed in the acetone solution containing DHA (0.05 mmol) and EB (0.5 mmol). The reaction mixture was stirred magnetically under pure oxygen (1 atm) or air atmosphere and sustained visible light irradiation, and the temperature of reaction solution increased to about 25 °C because of the heating effect of light irradiation. After the desired irradiation time had elapsed, the reaction was stopped and the oxidative products of EB were quantitatively analyzed on an Agilent 6890 N gas chromatograph (GC) with a DB-17 polysiloxane capillary column (30 m × 0.32 mm × 0.50 μm) and flame ionization detector (FID) using cyclohexanone as an internal standard, the oxidative products of DHA were determined on an Agilent 1260 HPLC (Agilent, USA) with an external standard method and the specific detection conditions were as follows: 4.6 × 250 mm of Agilent SB-C 18 chromatographic column, acetonitrile/ water 65:35 (v/v) of mobile phase, 0.5 mL/min of flow rate, 260 nm UV detector, column temperature 30 °C, injection volume 20 μL. The conversion of EB was calculated by dividing the actual added molar mass of EB by the reacted molar mass of EB obtained from the oxygenated products. The selectivity of ACP was calculated by dividing the molar mass of oxygenated products by the molar mass of ACP. The yield of AQ was calculated by dividing the actual produced molar mass of AQ by the theoretical molar mass of AQ.
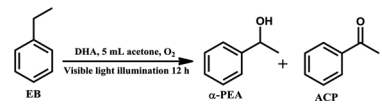
## Results and discussion

### Photooxidation of EB under different conditions

Table 2 lists the data for the DHA-triggered EB photooxidation to ACP under various reaction conditions. Under the standard conditions, with acetone solvent, 1 atm pure $O_2$ and 12 h of sustained visible light irradiation under room temperature, the DHA-based photosynthetic protocol could achieve 87.7 % EB conversion and 99.5 % selectivity (**Entry 1**), representing a mild and efficient character. Even if using air instead of pure $O_2$, the protocol still exhibited a good efficiency, affording 62.9 % EB conversion and 86.4 % ACP selectivity (**Entry 2**). And the use of AQ instead of DHA might achieve 86.5 % EB conversion

**Table 2**
The photooxidation of EB by molecular oxygen under different conditions.



| Entry | Change from standard conditions | Conv. (%) | Sel. (%) | | AQ yield (%) |
|---|---|---|---|---|---|
| | | | ACP | α-PEA | |
| 1 | Standard [a] | 87.7 | 99.5 | 0.5 | 71.8 |
| 2 | Air instead of $O_2$ | 62.9 | 96.3 | 3.7 | 56.7 |
| 3 | AQ instead of DHA | 86.5 | 99.8 | 0.2 | – |
| 4 [b,d] | Violet light, 6 h | 1.0 | 60.3 | 29.7 | 24.4 |
| 5 [b,c] | Blue light, 6 h | 0 | 0 | 0 | 0 |
| 6 [b,d] | Violet light, 6 h, AQ instead of DHA | 12.6 | 76.6 | 23.4 | – |
| 7 [b,c] | Blue light, 6 h, AQ instead of DHA | 0 | 0 | 0 | – |
| 8 [e] | Without light illumination | 0 | 0 | 0 | 0 |
| 9 | Without DHA | 0 | 0 | 0 | – |
| 10 | $N_2$ instead of $O_2$ | 0.1 | 36.1 | 63.9 | 0.8 |

[a]Standard reaction conditions: EB, 0.5 mmol; DHA, 0.05 mmol; Pure $O_2$, 1 atm; Acetone, 5 mL; 35 W tungsten-bromine lamp as a built-in light source, illumination time, 12 h; [b] By use of an external radiation; [c] Using a monochromatic green light with a center wavelength of 500 nm obtained by a 300 W xenon lamp equipped with a light filter of 500 nm; DHA, 0.4 mmol; Acetone, 20 mL; [d] Using a monochromatic violet light with a center wavelength of 400 nm obtained by a 300 W xenon lamp equipped with a light filter of 400 nm; DHA, 0.4 mmol; Acetone, 20 mL; [e] 35 °C, in the dark;

and 99.8 % ACP selectivity (**Entry 3**), which was almost equal to the current standard synthesis protocol. The current photooxidation was further studied with a monochromatic visible light as an external illumination to make clear the specific work wavelength (the reaction device sees Fig. S3). As shown in **Entry 4**, the auto-photooxidation of DHA by $O_2$ could be driven by a violet light of 400 nm and achieved 24.4 % AQ yield, along with the occurrence of a trace EB photooxidation (1% conversion). And AQ more efficiently catalyzed the photooxidation of EB with $O_2$ under this violet light illumination, providing a much higher 12.6 % EB conversion than the DHA-triggered EB photooxidation (**Entry 5**). But the photooxidation of EB by $O_2$ could not occur under the illumination of a blue light of 500 nm whether DHA or AQ was used as a source of photo-catalyst or a photo-catalyst (**Entries 6 and 7**). These findings indicate that DHA-triggered EB photooxidation can function only using a violet light part of tungsten-bromine lamp and its goal product AQ can work well owing to its stronger absorption to this violet light than DHA, as supported by UV–vis spectral characterizations in Fig. S4. Notably, AQ can be accumulated by preferentially catalyzing the photooxidation of DHA because the C–H bond dissociation energy (78.0 kcal● $mol^{-1}$) of DHA is smaller than that of EB (87 kcal● $mol^{-1}$). And the accumulated AQ, as an active photo-catalyst, should be responsible for the photooxidation of EB to ACP. Three blank experiments conducted in the absence of $O_2$ or DHA or without light irradiation confirmed that $O_2$, DHA and light irradiation are necessary for this photo-synthetic protocol (**Entries 8 and 10**).

### Photooxidation of various substrates

In order to verify the adaptability of the above DHA-based photosynthetic protocol, the photooxidation of various hydrocarbons with primary or/and secondary C–H bonds as well as four alcohols and a thioether was examined using the above standard reaction conditions. As shown in Table 3, in the examined hydrocarbons with secondary C–H bonds, DHA could very efficiently trigger the photo-oxidations of three aromatic EB, tetrahydronaphthalene and diphenylmethane, respectively affording 87.7, 90.2 and 97.5 % conversions with an almost 100 % selectivity for the corresponding ketones (**Entries 1-3**). But its synthetic efficiency was significantly reduced when *p*-bromoethylbenzene, especially cyclohexene and cyclohexane were used as substrates (**Entries 4-6**). **Entries 7–10** show that in the presence of DHA, benzyl alcohol, *n*-hexanol, especially cyclohexanol and thioanisole were also efficiently oxidized by $O_2$ to the corresponding oxygenated products under illumination, giving 71.4, 79.9, 94.8 and 96.5 % conversions, respectively. But DHA exhibited a relatively low efficiency for the photooxidation of furfuryl alcohol (**Entry 11**, 48.0 % conversion). **Entry 12** shows that with DHA, the photooxidation of toluene to benzaldehyde and benzoic acid could also proceed but afforded a low conversion of 24 %. And its reactivity was influenced by the aromatic ring substituent, which was significantly improved when introducing a *p*-methyl (**Entry 13**, 66.1 % conversion) but significantly decreased when introducing a *meso*-chlorine (**Entry 14**, 10 % conversion) and almost lost when introducing a *para*-NO_2 (**Entry 15**, 1% conversion). In addition, DHA exhibited a poor synthetic efficiency for the photooxidation of 2-methylfuran to furfural and furanoic acid (**Entry 16**, 10.3 % conversion) and was even completely ineffective for the photooxidation of *n*-pentane although this linear alkane contained secondary C–H bonds (**Entry 17**). The reactivity of some hydrocarbons diphenylmethane, tetrahydronaphthalene, EB, toluene and cyclohexane is obviously inversely proportional to their C–H bond dissociation energies (BDEs) at the reactive sites (see Table 3), supporting that their photo-activation complies with a hydrogen atom transfer (HAT) mechanism [36,37]. But the photo-activation of other hydrocarbons does not seem to comply with the HAT mechanism because the above-mentioned inverse relationship is controversial on them. Four typical examples are that *p*-xylene, toluene, *p*-nitrotoluene and *n*-pentane have almost equivalent BDE values at the reactive sites to each other, but

**Table 3**
Data for photooxidation of different substrates triggered by DHA auto-photooxidation [a].

| Entry | Substrate | Conv. (%) | Sel. of main products (%) | | | | | | | BDE [m] / kcal mol⁻¹ |
|---|---|---|---|---|---|---|---|---|---|---|
| 1 [b] | [structure] | 87.7 | [structure] 0.5 | | | [structure] 99.5 | | | | 87 [45] |
| 2 [c] | [structure] | 90.2 | [structure] 99.2 | | | [structure] 0.8 | | | | 85 [46] |
| 3 [d] | [structure] | 97.5 | [structure] 0 | | | [structure] 100 | | | | 82 [47] |
| 4 [d] | [structure] | 66.1 | [structure] 12.2 | | | [structure] 87.8 | | | | |
| 5 [e] | [structure] | 20.3 | [structure] 22.1 | | [structure] -OH 20.6 | [structure] =O 57.3 | | | | 84 [48] |
| 6 [f] | [structure] | 19.2 | [structure] -OH 12.2 | | | [structure] =O 87.8 | | | | 99 [49] |
| 7 [b] | [structure] -OH | 71.4 | [structure] CHO 65.1 | | | [structure] COOH 34.9 | | | | 83 [50] |
| 8 [e] | [structure] -OH | 79.9 | [structure] 11.2 | | | [structure] -OH 88.8 | | | | 92 [51] |
| 9 [f] | [structure] -OH | 94.8 | [structure] =O 100 | | | | | | | 91 [50] |
| 10 [c] | [structure] -S- | 96.5 | [structure] 89.8 | | | [structure] 10.2 | | | | |
| 11 [b] | [structure] -OH | 48.0 | [structure] 5.0 | | | [structure] -OH 95.0 | | | | |
| 12 [b] | [structure] | 24.0 | [structure] CHO 61.1 | | | [structure] COOH 38.9 | | | | 91.1 [41] |
| 13 [d] | [structure] | 66.1 | TPA [g] 2.8 | 4-CBA [h] 3.9 | TPD [i] 1.2 | p-TA [j] 83.1 | TALD [k] 9.0 | | | 90.7 [41] |
| 14 [d] | [structure] -Cl | 10.0 | [structure] 70.8 | | | [structure] 29.2 | | | | 90.8 [41] |
| 15 [d] | [structure] -NO₂ | 1.0 | [structure] -NO₂ 88.3 | | | [structure] -NO₂ 11.7 | | | | 90.5 [41] |
| 16 [b] | [structure] | 10.3 | [structure] 1.7 | | | [structure] 98.3 | | | | 89 [52] |
| 17 [l] | [structure] | 0 | [structure] 0 | [structure] -OH 0 | | [structure] 0 | [structure] -OH 0 | | | 94 [51] |

[a] Reaction condition: Substrate, 0.5 mmol; DHA, 0.05 mmol; Pure $O_2$, 1 atm; Acetone, 5 mL; 35 W tungsten-bromine lamp as a built-in light source, illumination time, 12 h. [b] The oxidative products were quantitatively analyzed on an Agilent 6890 N gas chromatograph (GC) using cyclohexanone as an internal standard; [c] The oxidation products were quantified by GC using anisole as an internal standard. [d] The oxidation products were quantified by Agilent 1260 HPLC with an external standard method; [e] The oxidation products were quantified by GC using EB as an internal standard. [f] The oxidation products were quantified by GC using cyclopentanone as an internal standard; [g] TPA denotes terephthalic acid; [h] 4-CBA denotes *p*-carboxybenzaldehyde; [i] TPD denotes *p*-phthalaldehyde; [j] *p*-TA denotes *p*-toluic acid; [k] TALD denotes *p*-tolu.aldehyde; [l] No product was detected by GC; [m] BDE denotes bond dissociation energy.

they are very different in reactivity. Notably, the reactivity of these four substrates is obviously inversely related to their ionization energies (IEs, 185, 194, 230 and 241 kcal mol⁻¹ [41,42]), supporting that their photo-activation likely relies on the electron transfer (ET) pathway, as previously suggested by Neumann and co-workers in the oxidation of toluene derivatives catalyzed by $H_5PV_2Mo_{10}O_{40}$ in 50 % $H_2SO_4$ solution [43]. In addition, the stability of carbon-centered radical generated in the photo-activation of hydrocarbons by HAT or ET-coupled proton transfer (ET−PT) pathway is dominated by spin delocalization [44], which may be the factor that determines the reactivity of hydrocarbons [43]. It is well known that benzylic radical has a higher stability than allyl and especially alkyl radicals, and its stability increases on the electron donating alkyl substituents but decreases on the electron withdrawing halogen substituents [42,43]. Therefore, the much higher reactivity of alkyl aromatics than the halogen- or especially nitro-substituted toluene derivatives and nonaromatic hydrocarbons is partly due to a good stability of their benzylic radicals.

*Effect of variables on DHA-triggered EB photooxidation*

The effect of variables on DHA-triggered EB photooxidation was further examined and the results are shown in Figs. 1–4. It can be seen from Fig. 1 that the efficiency of EB photooxidation triggered by DHA was drastically influenced by reaction medium, which was the highest in acetone medium with a good solubility for the actual photo-generated catalyst AQ. However, the efficiency was remarkably reduced in MeCN, providing only 45.9 % EB conversion and 67.7 % ACP selectivity. One possible reason is that AQ is low soluble in MeCN and its continuous accumulation during photoreaction causes the reaction solution become very turbid, thus leading to a significant decrease of light absorption efficiency. It is puzzling that in DMF or DMA, it was almost
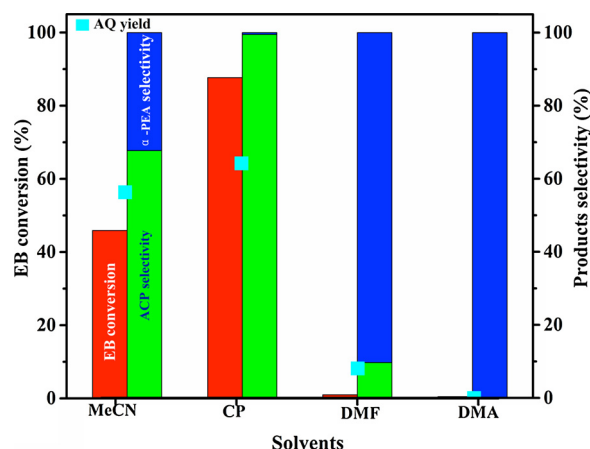


**Fig. 1.** Effect of solvents on the DHA-mediated ethylbenzene photooxidation (By use of standard reaction conditions in Table 2 except for solvent).

or completely impossible to trigger EB photooxidation by DHA although these two solvents had a better solubility for AQ than acetone. We propose from these solvents-regulated AQ yields in Fig. 1, that the efficiency of DHA auto-photooxidation to AQ in these solvents should be mainly responsible for that of EB photooxidation. And photoluminescence spectra of DHA in these solvents shown in Fig. S5 and the control experiments with DMA and DMF as additives in Table S1, support that the favorable solvation effect of MeCN and especially acetone should originate from that they may stabilize the photo-excited state of DHA but also hardly affect the activity of superoxide free radical ($O_2^{\bullet-}$) generated in photoreaction. In sharp contrast, the
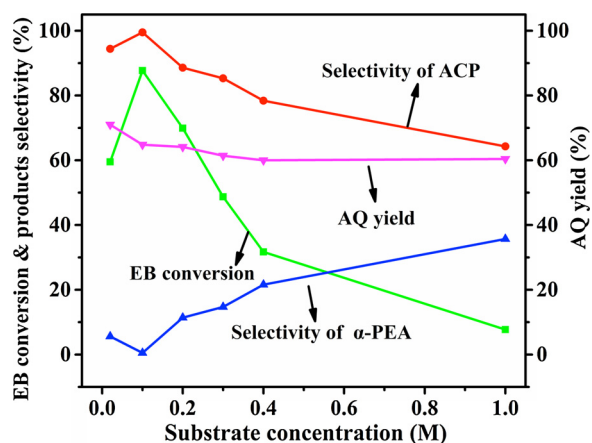
**Fig. 2.** Effect of substrate EB concentration on its photooxidation (By use of standard reaction conditions in Table 2 except for ethylbenzene concentration).
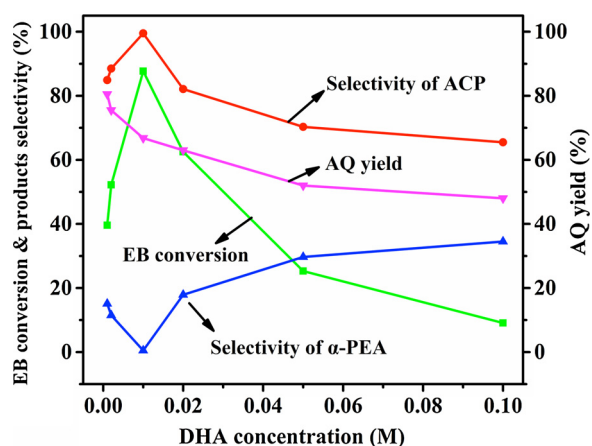


**Fig. 3.** Effect of DHA concentration on its-mediated photooxidation of ethylbenzene (By use of standard reaction conditions in Table 2 except for DHA concentration).



**Fig. 4.** Effect of illumination time on the photooxidation of EB in the presence of DHA (a) or AQ (b).
(By the use of standard reaction conditions in Table 2).

inertness of DMF and especially DMA in auto-photooxidation of DHA should be mainly due to their significantly deactivating and even quenching effect on the $O_2^{\bullet-}$ radical except partly due to their weaker stabilizing effect on the excited state of DHA.

Fig. 2 illuminates the influence of substrate EB concentration on its photooxidation by $O_2$ in acetone. In that, when the concentration of EB was enhanced from 0.02 to 0.1 M, its conversion continuously and rapidly increased from 59.5–87.7%, along with a gradual increase in ACP selectivity, from 94.4–99.5%. Thereafter, a further enhancing the concentration from 0.1 to 1.0 M resulted in a drastic reduction in the conversion from 87.7 to 7.7 %, along with a decrease in ACP selectivity from 99.5–64.3%. The yield of AQ in this photosynthetic protocol continuously decreases to about 61.4 % with increasing EB concentration from 0.02 to 0.3 M, and then remains substantially unchanged when further enhancing EB concentration. The abnormal photooxidation efficiency at low EB concentration may be because when the concentration of EB decreases to equal that of DHA, the AQ-based photocatalytic oxidation, as supported by the yield curve of AQ in Fig. 2, occurs upon DHA with high probability as DHA has a higher reactivity than EB. On the other hand, the collision probability between the catalyst AQ and the substrate EB is also reduced at low EB concentration. Here, the optimal concentration of EB was 0.1 M.

Fig. 3 illuminates the influence of DHA concentration on its mediated photooxidation of EB by $O_2$ in acetone. As expected, when the concentration of DHA was enhanced from 0.001 to 0.01 M, the conversion of EB continuously and rapidly increased from 39.6–87.7%,
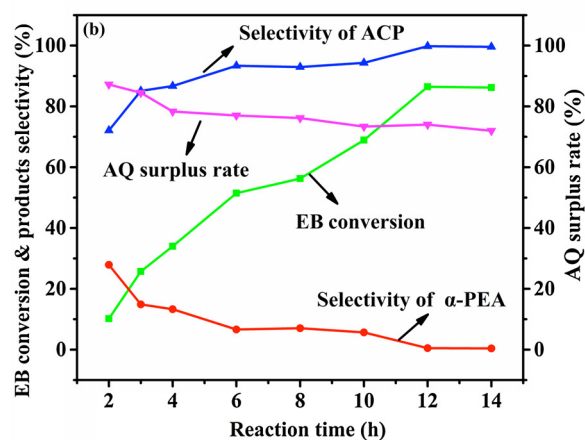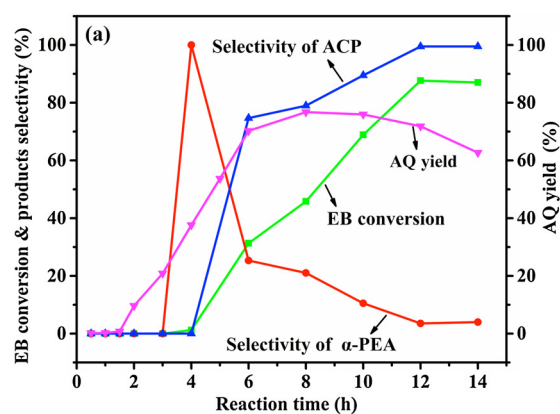
along with a gradual increase in ACP selectivity, from 84.9–99.5%. Thereafter, a further enhancing DHA concentration from 0.01 to 0.10 M resulted in a drastic reduction in EB conversion from 87.7–9.1%, along with a decrease in ACP selectivity from 99.5–65.5%. At the same time, the conversion efficiency of DHA to AQ decreased continuously with enhancing its concentration. The abnormal photosynthetic efficiency of this protocol at high DHA concentration may be due to the two following reasons: The photooxidation of DHA catalyzed by the AQ in situ generated preferentially proceeds owing to its higher reactivity than EB, and this advantage is magnified at a high DHA concentration. On the other hand, a large number of precipitated AQ solid generated during photooxidation of high-concentration DHA seriously affects the transmittance of visible light, thus leading to a significant reduction in the efficiency of EB photooxidation.

Fig. 4a and b compare the effects of irradiation time on the photooxidation of EB by $O_2$ in acetone using the DHA-based photosynthetic protocol and AQ photocatalyst, respectively. As shown in Fig. 4a, DHA could not trigger the photooxidation of EB at the beginning of the reaction ($0-3$ h), indicating the existence of induction period. But the auto-photooxidation of DHA could proceed at this stage, affording 20.8 % AQ yield. After that, the photooxidation of EB proceeded very slowly at $3-4$ h, providing a poor 3.2 % conversion and α-phenylethanol as the only oxygenated product. In the middle to late stages of EB photooxidation ($4-12$ h), EB conversion and ACP selectivity were continuously and rapidly enhanced with the time, from 3.2%–87.6% and from 0 to 99.8 %, respectively, along with a significant increase of AQ yield from 37.6 and 71.8 %. After 12 h, the effect of irradiation time on the photooxidation of EB was almost negligible. Fig. 4b shows that when AQ was directly used as a photo-catalyst, the induction period

above-described could be eliminated completely. the conversion of EB uninterruptedly and quickly increased with the time in the whole period of reaction, along with a continuous increase in the yield and selectivity of ACP. Furthermore, the photocatalytic efficiency of AQ for EB oxidation to ACP was higher than that of the DHA-based photo-synthetic protocol in the reaction stage of $4-10$ h, but tended to agree with each other in the final reaction stage. These findings support that in the early reaction period, DHA is slowly photo-oxidized to its target product AQ. In the mid-reaction, the generated AQ, as an active pho-tocatalyst, can continuously and significantly accelerate the photo-oxidation of DHA owing to a gradual accumulation of AQ, along with the occurrence and acceleration of EB photooxidation. Because DHA has a lower concentration and higher reactivity than EB, its complete conversion to AQ can be achieved at this stage, as supported by the auto-photooxidation results of DHA in the absence of EB (See Fig. S6). In the late reaction, the highly accumulated AQ is fully involved in the photooxidation of EB (See Fig. S7), finally affording 87.7 % EB con-version and 99.8 % ACP selectivity at 12 h.

## Proposed photooxidation mechanism for synthesis of ACP from EB

### Quenching experiments of active species

In order to explore the mechanism of photooxidation of EB driven by DHA auto-photooxidation, the possible photo-generated active spe-cies in the DHA-based photo-synthetic protocol were examined by a series of quenching experiments. As shown in Fig. 5, the photooxidation of EB with $O_2$ could still proceed after the addition of sodium oxalate ($Na_2C_2O_4$, a quencher of oxygen vacancies, hole $h^+$), benzoquinone (BQ, a quencher of $O_2^{-\bullet}$), especially isopropanol (IPA, a quencher of $\bullet OH$) [2,53–57] although its conversion was decreased to some extent compared to that obtained without any scavengers. But EB photo-oxidation was almost completely quenched by TEMPO (a quencher of all free radicals [58]). Notably, the above quenching effects were also noticed upon the AQ-directly catalyzed EB photooxidation with $O_2$ (See Fig. S8). These findings suggest that the photo-generated oxygen va-cancies (holes) and photoelectrons-derived $O_2^{-\bullet}$ by the excitation of AQ under visible light in the DHA-based photosynthetic protocol should be responsible for the photooxidation of EB. Based on the quenching experiment of IPA, the radical species $\bullet OH$ seems to be involved in the current photooxidation protocol, but this speculation can be excluded completely according to a fact that the quenching effect of IPA on the auto-photooxidation of DHA to AQ was almost negligible (see Fig. S9). We guess that IPA, as an active substrate, may participate in the com-petition of photooxidation with EB and its second C–H BDE ($90.6$ kcal mol$^{-1}$ [51]) is only higher than that of EB, so that its addition
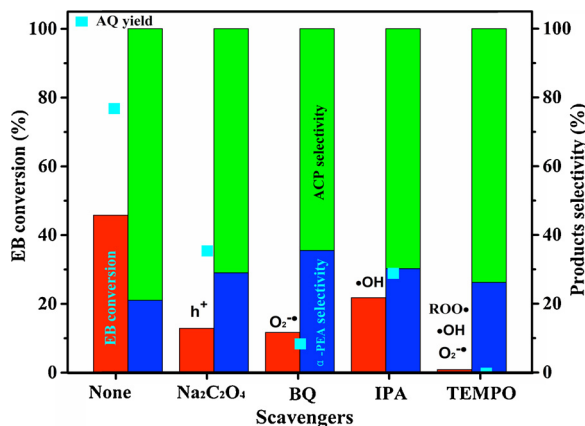
**Fig. 5.** The effect of various scavengers on the photooxidation of EB driven by DHA photo-auto-oxidation.
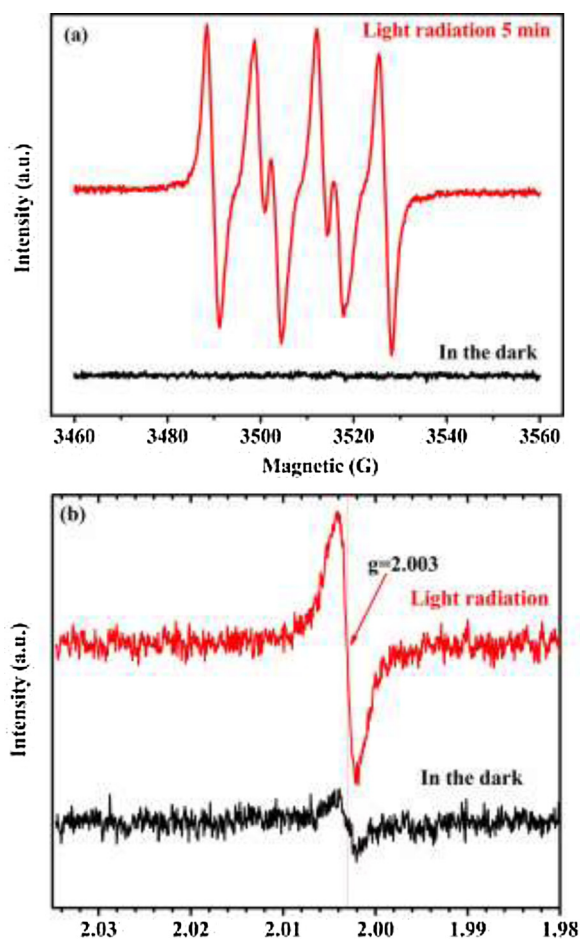Reaction conditions: 0.05 mmol DHA, 0.5 mmol EB, 5 ml acetone, 0.6 mmol quencher, 1 atm $O_2$, illumination 8 h;

**Fig. 6.** EPR spectra of TMPO-captured $O_2^{\cdot-}$ (a) and photo-excited AQ (b) in acetone under visible light.

leads to a reduction in an efficiency of EB photooxidation. Additionally, the contribution of singlet oxygen ($^1O_2$) to the current photooxidation was further confirmed by the following control experiment. As shown in Table S2, the deuterated acetone was used as a reaction medium to enhance the stability of $^1O_2$ [59,60], the DHA-triggered EB photo-oxidation could proceed more efficiently and EB conversion increased ca. 6% compared to that obtained in acetone, which in consistence with the result previously reported in the AQ-based photooxidation system [61].

### EPR spin trapping

EPR spectrum is a powerful tool to certify the existence of super-oxide radical anion ($O_2^{\cdot-}$) and oxygen vacancies (holes, $h^+$) [62,63], which was applied to the current photooxidation system. The capturing of $O_2^{\cdot-}$ radical anion with DMPO (50 mM) and the generation of $h^+$ species in the AQ-based photo-catalytic system were performed in acetone under visible light and $O_2$ atmosphere. The AQ solution was stirred for 5 min with or without illumination and immediately trans-ferred to a test tube and its EPR signal measured under normal condi-tions. As shown in Fig. 6a, no any EPR signal was observed when the capturing experiment was performed in the dark. However, the DMPO-$O_2^{\cdot-}$ EPR signal could be found clearly under visible light illumination, providing a direct proof that $O_2^{\cdot-}$, as the important active oxygen species, exists in the photooxidation protocol, which is accordant with the results reported by other authors [64–67]. Fig. 6b displays that the EPR signal of AQ in acetone was almost silent without light illumination but an apparent symmetrical signal at g = 2.003 appeared in its EPR spectrum under visible light illumination, which can be assigned to the
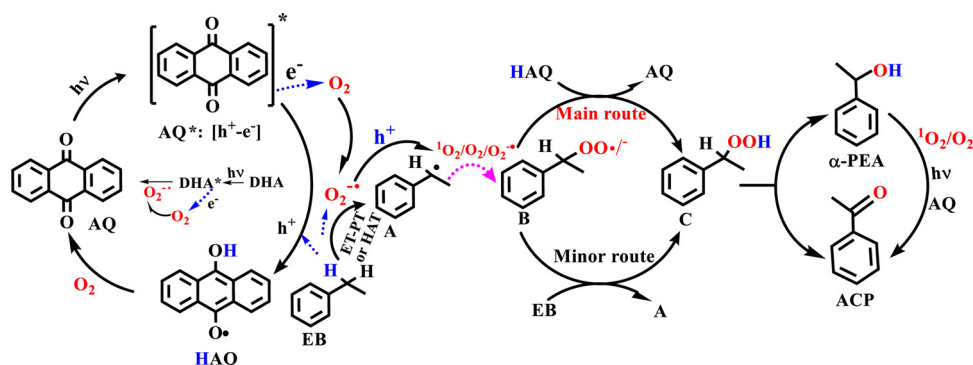
**Scheme 1.** mechanism of EB oxidation catalyzed by AQ with $O_2$ under visible light.

oxygen vacancies with spin electrons [63]. The above EPR results clearly certificate the existence of two active species $O_2^{\cdot-}$ and $h^+$ in the AQ catalysis system derived by DHA auto-photooxidation, which co-incides with the quenching experiments of active species.

*Proposed photooxidation mechanism*

According the present results and the previous literature reports [68–72], we propose that DHA is excited to generate its photo-excited state (DHA*) under visible light illumination, as supported by UV–vis and PL spectra in Figs. S4 and S5. Then, the reductive photo-electrons of DHA* may be transferred to $O_2$, generating superoxide radical anions ($O_2^{-\bullet}$), as supported by the radical quenching experiments and EPR spectrum of the DMPO-captured $O_2^{-\bullet}$ radicals in DHA photo-auto-oxidation system (Figs. S10 and S11). The $O_2^{-\bullet}$ radicals, as active oxygen species, should be responsible for the auto-photooxidation of DHA to AQ, as an actual photo-catalyst in the current photo-synthetic protocol. Next, a possible mechanism for EB photooxidation to ACP catalyzed by the in situ generated and continuously accumulated AQ from DHA auto- photooxidation under visible light and $O_2$ atmosphere is proposed as follows (Scheme 1): AQ can be excited by visible light to generate its photo-generated oxygen vacancies ($h^+$)-electrons ($e^-$) pairs (excite state, AQ*), supported by the UV–vis, PL and EPR spectra of AQ in acetone (Figs. S4 and S11 and Fig. 6b). The photoelectrons of AQ*, as supported by the above EPR spectrum in Fig. 6a, can rapidly be transferred to $O_2$, thus reducing the recombination of photo-generated charges pairs ($h^+$-$e^-$) and generating the active $O_2^{\cdot-}$ radical anions. Then, the strong oxidative $h^+$ species, likely including $O_2^{\cdot-}$, can oxidize the benzyl C–H bond of EB to yield the reduced AQ (HAQ) and the benzyl radical (A) *via* HAT [36,37] or ET−PT (main pathway) [43] mechanism. In addition, the formation of $^1O_2$ is attributed to the interactions between $O_2^{\cdot-}$ and VB holes [73]. Then, the radical A combines with $^1O_2/O_2$ or $O_2^{\cdot-}$ to form its peroxy radical or anion (B), and the latter is more likely to deprive one H atom of the reduced catalyst HAQ, thus (re)generating its hydroperoxide (C) and the starting AQ (photo-catalysis cycling pathway) [40]. Finally, the species C can be converted to form the corresponding α-PEA and ACP, α-PEA may be further oxidized to ACP by the above photocatalytic route. Of course, an auto-oxidation route that benzyl radical chains are propagated by reaction of the species B with another EB, as a minor pathway, may also exists in the current photooxidation and is described in Scheme 1. In this case, the regeneration of catalyst can be achieved using $O_2$ as an oxidant.

## Conclusion

In summary, a mild and efficient photooxidation protocol has been developed to synthesize ACP from EB and its outstanding advantages, which can fully reflect the principle of green chemistry, are summarized as follows: 1) Using inexpensive, readily available DHA, visible light

and $O_2$/air as a catalyst source, an illumination source and a green oxidant, respectively; 2) Mild reaction conditions, easy to operate; 3) Achieving a 87.7 % EB conversion and 99.5 % ACP selectivity; 4) Having a good adaptability for the photooxidation of other compounds such as alkylbenzene, cyclohexane, alcohols, thioethers, and olefins. Based on an efficient photo-catalytic performance of AQ derived from this photooxidation protocol, we are interested in further exploring the use of AQ and it's derives to highly-efficiently achieve the photo-oxidation of organic compounds with $O_2$.

## CRediT authorship contribution statement

## Declaration of Competing Interest

The authors declare that they have no known competing financial interests or personal relationships that could have appeared to influence the work reported in this paper.

## Acknowledgements

## Appendix A. Supplementary data

Supplementary material related to this article can be found, in the online version, at doi:https://doi.org/10.1016/j.mcat.2020.111127.

## References

[1] W.L. Guo, Z.H. Zhang, H. Lin, L. Cai, Z-scheme BiFeO₃-CNTs-PPy as a highly effective and stable photocatalyst for selective oxidation of benzyl alcohol under

visible-light irradiation, Mol. Catal. 492 (2020) 111011.

[2] M. Mohammadi, H. Hadadzadeh, M. Kaikhosravi, H. Farrokhpour, J. Shakeri, Selective photocatalytic oxidation of benzyl alcohol at ambient conditions using spray-dried g-C₃N₄/TiO₂ granules, Mol. Catal. 490 (2020) 110927.

[3] A. Selvamani, M. Selvaraj, P.S. Krishnan, M. Gurulakshmi, K. Shanthi, Low temperature vapor phase selective oxidation of ethylbenzene over Ce₁₋ₓ MnₓO₂ nanocubes, Appl. Catal. A-Gen. 495 (2015) 92–103.

[4] W. Lv, L. Yang, B. Fan, Y. Zhao, Y. Chen, N. Lu, R. Li, Silylated MgAl LDHs intercalated with MnO₂ nanowires: highly efficient catalysts for the solvent-free aerobic oxidation of ethylbenzene, Chem. Eng. J. 263 (2015) 309–316.

[5] H. Li, H. Ma, X. Wang, J. Gao, C. Chen, S. Shi, M. Qu, N. Feng, J. Xu, Efficient oxidation of ethylbenzene catalyzed by cobalt zeolitic imidazolate framework ZIF-67 and NHPI, J. Energy Chem. 23 (2014) 742–746.

[6] G. Huang, C. Yan, J.L. Cai, L.Q. Mo, S.K. Zhao, Y.A. Guo, S.J. Wei, Y.L. Shen, Practicably efficient ethylbenzene oxidation catalyzed by manganese tetrakis(4-sulfonatophenyl)porphyrin grafted to powdered chitosan, J. Porphyr. Phthalocya. 22 (2018) 481–490.

[7] R. Maheswari, M.P. Pachamuthu, R. Anand, Copper containing TUD-1: synthesis, characterization and catalytic behavior in liquid-phase oxidation of ethylbenzene, J. Porous Mat. 19 (2011) 103–110.

[8] M. Arshadi, M. Ghiaci, Highly efficient solvent free oxidation of ethylbenzene using some recyclable catalysts: the role of linker in competency of manganese nanocatalysts, Appl. Catal. A-Gen. 399 (2011) 75–86.

[9] D. Habibi, A.R. Faraji, Synthesis, characterization and application of a nano-manganese-catalyst as an efficient solid catalyst for solvent free selective oxidation of ethylbenzene, cyclohexene, and benzylalcohol, Appl. Surf. Sci. 276 (2013) 487–496.

[10] D. Habibi, A.R. Faraji, M. Arshadi, H. Veisi, A. Gil, Manganese nanocatalyst and N-hydroxyphthalimide as an efficient catalytic system for selective oxidation of ethylbenzene, cyclohexene and oximes under aerobic condition, J. Mol. Catal. A-Chem. 382 (2014) 41–54.

[11] X. Lin, S.S. Jie, Z.G. Liu, Sulfur and nitrogen-doped porous cobalt carbon catalyst for high efficient aerobic oxidation of hydrocarbons, Mol. Catal. 455 (2018) 143–149.

[12] S.S. Jie, C.Q. Yang, Y. Chen, Z.G. Liu, Facile synthesis of ultra-stable Co-N-C catalysts using cobalt porphyrin and peptides as precursors for selective oxidation of ethylbenzene, Mol. Catal. 458 (2018) 1–8.

[13] M. Nasrollahzadeh, Z. Nezafat, N.S.S. Bidgoli, N. Shafiei, Recent progresses in polymer supported cobalt complexes/nanoparticles for sustainable and selective oxidation reactions, Mol. Catal. 484 (2020) 110775.

[14] K. Xavier, Zeolite-encapsulated Co(II), Ni(II) and Cu(II) complexes as catalysts for partial oxidation of benzyl alcohol and ethylbenzene, Appl. Catal. A-Gen. 258 (2004) 251–259.

[15] T. Chakrabortya, A. Chakrabortya, S. Maityb, D. Dasa, T. Chattopadhyay, Conglomerated system of Ag nanoparticles decorated Al₂O₃ supported cobalt and copper complexes with enhanced catalytic activity for oxidation reactions, Mol. Catal. 462 (2019) 104–113.

[16] S. Dapurkar, H. Kawanami, T. Yokoyama, Y. Ikushima, Solvent-free selective oxidation of benzylic compounds over chromium containing mesoporous molecular sieve catalyst at 1atm O₂, Catal. Commun. 10 (2009) 1025–1028.

[17] K.M. Parida, S.S. Dash, Manganese containing MCM-41: synthesis, characterization and catalytic activity in the oxidation of ethylbenzene, J. Mol. Catal. A-Chem. 306 (2009) 54–61.

[18] S. Vetrivel, A. Pandurangan, Vapour-phase oxidation of ethylbenzene with air over Mn-containing MCM-41 mesoporous molecular sieves, Appl. Catal. A-Gen. 264 (2004) 243–252.

[19] S.S. Bhoware, S. Shylesh, K.R. Kamble, A.P. Singh, Cobalt-containing hexagonal mesoporous molecular sieves (Co-HMS): synthesis, characterization and catalytic activity in the oxidation reaction of ethylbenzene, J. Mol. Catal. A-Chem. 255 (2006) 123–130.

[20] S. Devika, M. Palanichamy, V. Murugesan, Selective oxidation of ethylbenzene over CeAlPO-5, Appl. Catal. A-Gen. 407 (2011) 76–84.

[21] S. Jana, Y. Kubota, T. Tatsumi, High activity of Mn-MgAl hydrotalcite in heterogeneously catalyzed liquid-phase selective oxidation of alkylaromatics to benzylic ketones with 1 atm of molecular oxygen, J. Catal. 247 (2007) 214–222.

[22] B. Monteiro, S. Gago, S.S. Balula, A.A. Valente, I.S. Gonçalves, M. Pillinger, Liquid-phase oxidation catalysed by copper(II) immobilised in a pillared layered double hydroxide, J. Mol. Catal. A-Chem. 312 (2009) 23–30.

[23] V. Choudhary, J. Indurkar, V. Narkhede, R. Jha, MnO₄⁻ exchanged Mg-Al hydrotalcite: a stable and reusable/environmental-friendly catalyst for selective oxidation by oxygen of ethylbenzene to acetophenone and diphenylmethane to benzophenone, J. Catal. 227 (2004) 257–261.

[24] R. Xie, G. Fan, L. Yang, F. Li, Hierarchical flower-like Co-Cu mixed metal oxide microspheres as highly efficient catalysts for selective oxidation of ethylbenzene, Chem. Eng. J. 288 (2016) 169–178.

[25] Q. Sun, X. Song, L. Gao, W. Chen, Y. Li, L. Mao, J.H. Yang, Heterogeneous liquid phase oxidation of ethylbenzene to acetophenone with graphene carbon-based catalyst, Chem. Pap. 72 (2018) 2203–2214.

[26] R. Xie, G. Fan, L. Yang, F. Li, Solvent-free oxidation of ethylbenzene over hierarchical flower-like core–shell structured Co-based mixed metal oxides with significantly enhanced catalytic performance, Catal. Sci. Technol. 5 (2015) 540–548.

[27] Y. Li, S. Jie, K. Li, Z. Liu, Synthesis of efficient Co and N co-doped carbon catalysts with high surface areas for selective oxidation of ethylbenzene, New J. Chem. 42 (2018) 12677–12683.

[28] Y. Zhao, R. Xie, Y. Lin, G. Fan, F. Li, Highly efficient solvent-free aerobic oxidation of ethylbenzene over hybrid Zn–Cr layered double hydroxide/carbon nanotubes nanocomposite, Catal. Commun. 114 (2018) 65–69.

[29] J. Luo, F. Peng, H. Yu, H. Wang, W. Zheng, Aerobic liquid-phase oxidation of ethylbenzene to acetophenone catalyzed by carbon nanotubes, ChemCatChem 5 (2013) 1578–1586.

[30] J. Qin, Z. Fu, Y. Liu, X. He, D. Zhang, W. Wu, Y. Wang, X. Gong, X. Deng, H. Wu, Y. Zou, N. Yu, D. Yin, Aerobic oxidation of ethylbenzene Co-catalyzed by N-Hydroxyphthalimide and oxobis(8-Quinolinolato) vanadium (IV) complexes, Chinese J. Catal. 32 (2011) 1342–1348.

[31] W. Zhou, X. Dai, Y. Chen, Fa. Sun, M. He, Q. Chen, Synergistic catalytic oxidation of ethylbenzene to acetophenone by metallophthalocyanine intercalated layered double hydroxide with oxygen, ChemistrySelect 3 (2018) 566–572.

[32] X.X. Zhao, Y. Zhang, P. We, G. Xu, D. Ma, P. Qiu, NH₂-MIL-125(Ti)/TiO₂ composites as superior visible-light photocatalysts for selective oxidation of cyclohexane, Mol. Catal. 452 (2018) 175–183.

[33] A. Akhundi, A. Badiei, G.M. Ziarani, A.H. Yangjeh, M.J.M. Batista, R. Luque, Graphitic carbon nitride-based photocatalysts: toward efficient organic transformation for value-added chemicals production, Mol. Catal. 488 (2020) 110902.

[34] S.G.H. Michael, A. Gonzalez, Subhas K. Sikdar, Photocatalytic Selective Oxidation of Hydrocarbons in the Aqueous Phase, J. Catal. 183 (1999) 159–162.

[35] S. Tang, W. Wu, Z. Fu, S. Zou, Y. Liu, H. Zhao, S.R. Kirk, D. Yin, Vanadium-substituted tungstophosphoric acids as efficient catalysts for visible-light-Driven oxygenation of cyclohexane by dioxygen, ChemCatChem 7 (2015) 2637–2645.

[36] B. Yang, Z. Fu, A. Su, J. She, M. Chen, S. Tang, W. Hu, C. Zhang, Y. Liu, Influence of tetraalkylammonium cations on quality of decatungstate and its photocatalytic property in visible light-triggered selective oxidation of organic compounds by dioxygens, Appl. Catal. B-Environ. 242 (2019) 249–257.

[37] A. Su, M. Chen, Z. Fu, B. Yang, J. She, F. Wan, C. Zhang, Y. Liu, Hybridizing engineering strategy of non-lacunary (ⁿBu₄N)₄W₁₀O₃₂ by carbon quantum dot with remarkably enhanced visible-light-catalytic oxidation performance, Appl. Catal. A-Gen. 587 (2019) 117261.

[38] B. Srinivas, P. Anil Kumar Reddy, P. Rajesh, V. Durga Kumari, M. Subrahmanyam, B.R. De, Selective solar photocatalytic oxidation of ethylbenzene on C, N, and S doped TiO₂, Res. Chem. Intermediat. 37 (2011) 901–918.

[39] D. Jiang, W. Hu, M. Chen, Z. Fu, A. Su, B. Yang, F. Mao, C. Zhang, Y. Liu, D. Yin, Visible-light-Triggered quantitative oxidation of 9,10-Dihydroanthracene to Anthraquinone by O₂ under mild conditions, ChemSusChem 13 (2020) 1785–1792.

[40] W. Wu, X. He, Z. Fu, Y. Liu, Y. Wang, X. Gong, X. Deng, H. Wu, Y. Zou, N. Yu, D. Yin, Metal chlorides-catalyzed selective oxidation of cyclohexane by molecular oxygen under visible light irradiation, J. Catal. 286 (2012) 6–12.

[41] T. Fox, P.A. Kollman, Calculation of ionization potentials and C–H bond dissociation energies of toluene derivatives, J. Phys. Chem. C 100 (1996) 2950–2956.

[42] Y.R. Luo, P.D. Pacey, Effects of alkyl substitution on ionization energies of alkanes and haloalkanes and on heats of formation of their molecular cations Part 2.* Alkanes and chloro-, bromo- and iodoalkanes, Int. J. Mass Spectrom. Ion Process. 112 (1992) 63–77.

[43] B.B. Sarma, I. Efremenko, R. Neumann, Oxygenation of methylarenes to benzaldehyde derivatives by a polyoxometalate mediated electron transfer-oxygen transfer reaction in aqueous sulfuric Acid, J. Am. Chem. Soc. 137 (2015) 5916–5922.

[44] Y.D. Wu, C.L. Wong, K.W.K. Chan, Substituent effects on the C–H bond dissociation energy of toluene. A density functional study, J. Org. Chem. 61 (1996) 746–750.

[45] J.R. Bryant, J.M. Mayer, Oxidation of C–H bonds by [(bpy)₂(py)RuⁱⱽO]²⁺ occurs by hydrogen atom abstraction, J. Am. Chem. Soc. 125 (2003) 10351–10361.

[46] K.O.T. Matsumoto, K. Honda, A. Yazawa, S.F.H. Furutachi, S. Fukuzumi, and M.Suzuki, Aliphatic C–H Bond Activation Initiated by a (μ-η²:η²-Peroxo)dicopper(II) Complex in Comparison with Cumylperoxyl Radical, J. Am. Chem. Soc. 131 (2009) 9258–9267.

[47] W.L. Man, W.W. Lam, H.K. Kwong, S.M. Peng, W.T. Wong, T.C. Lau, Reaction of a (Salen)ruthenium(VI) nitrido complex with thiols. C–H bond activation by (Salen) ruthenium(IV) sulfilamido species, Inorg. Chem. 49 (2010) 73–81.

[48] S.L. Khursan, D.A. Mikhailov, V.M. Yanborisov, D.I. Borisov, AM1 calculations of bond dissociation energies. Allylic and benzylic C–H bonds, React. Kinet. Catal. Lett. 61 (1997) 91–95.

[49] D. Dhar, W.B. Tolman, Hydrogen atom abstraction from hydrocarbons by a copper (III)-Hydroxide complex, J. Am. Chem. Soc. 137 (2015) 1322–1329.

[50] J. Xie, P.K. Lo, C.S. Lam, K.C. Lau, T.C. Lau, A hydrogen-atom transfer mechanism in the oxidation of alcohols by [FeO₄]²⁻ in aqueous solution, Dalton Trans. 47 (2017) 240–245.

[51] K.K. Timergazin, S.L. Khursan, Quantum-chemical calculations of the dissociation energy of the C–H bond in hydrocarbons, alcohols, and ethers, Russ. Chem. Bull. 45 (1996) 2858–2861.

[52] S.W. Zhao, L. Liu, Y. Fu, Q.X. Guo, Assessment of the metabolic stability of the methyl groups in heterocyclic compounds using C–H bond dissociation energies: effects of diverse aromatic groups on the stability of methyl radicals, J. Phys. Org. Chem. 18 (2005) 353–367.

[53] Y. Shiraishi, S. Shiota, H. Hirakawa, S. Tanaka, S. Ichikawa, T. Hirai, Titanium Dioxide/Reduced graphene oxide hybrid photocatalysts for efficient and selective partial oxidation of cyclohexane, ACS Catal. 7 (2016) 293–300.

[54] Y. Shiraishi, Y. Sugano, S. Ichikawa, T. Hirai, Visible light-induced partial oxidation of cyclohexane on WO₃ loaded with Ptnanoparticles, Catal. Sci. Technol. 2 (2012) 400–405.

[55] Q. Wu, Y.M. He, H.L. Zhang, Z.Y. Feng, Y. Wu, T.H. Wu, Photocatalytic selective oxidation of biomass-derived 5-hydroxymethylfurfural to 2,5-diformylfuran on metal-free g-C₃N₄ under visible light irradiation, Mol. Catal. 436 (2017) 10–18.

[56] J.P. Zou, D.D. Wu, J. Luo, Q.J. Xing, X.B. Luo, W.H. Dong, S.L. Luo, H.M. Du, S.L. Suib, A strategy for one-pot conversion of organic pollutants into useful hydrocarbons through coupling photodegradation of MB with photoreduction of CO₂,

ACS Catal. 6 (2016) 6861–6867.

[57] W.H. Dong, D.D. Wu, J.M. Luo, Q.J. Xing, H. Liu, J.P. Zou, X.B. Luo, X.B. Min, H.L. Liu, S.L. Luo, C.T. Au, Coupling of photodegradation of RhB with photo-reduction of $CO_2$ over rGO/$SrTi_{0.95}Fe_{0.05}O_{3-\delta}$ catalyst: A strategy for one-pot conversion of organic pollutants to methanol and ethanol, J. Catal. 349 (2017) 218–225.

[58] I. Cosemans, L. Hontis, D. Van Den Berghe, A. Palmaerts, J. Wouters, T.J. Cleij, L. Lutsen, W. Maes, T. Junkers, D.J.M. Vanderzande, Discovery of an anionic polymerization mechanism for high molecular weight PPV derivatives via the sulfinyl precursor route, Macromolecules 44 (2011) 7610–7616.

[59] R. Rahal, M.L. Bechec, R. Guyoneaud, T. Pigot, H. Paolacci, S. Lacombe, Bactericidal activity under UV and visible light of cotton fabrics coated with anthraquinone-sensitized $TiO_2$, Catal. Today 209 (2013) 134–139.

[60] M.D. Maree, N. Kuznetsova, T. Nyokong, Silicon octaphenoxyphthalocyanines: photostability and singlet oxygen quantum yields, J. Photochem. Photobio. A: Chem. 140 (2001) 117–125.

[61] G. Bracchitta, A. Catalfo, G. De Guidi, Photoinduced protein modifications by methylene blue and naproxen, Photochem. Photobiol. Sci. 11 (2012) 1886–1896.

[62] J.P. Campbell, P.M. Lenahan, C.J. Cochrane, A.T. Krishnan, S. Krishnan, Atomic-scale defects involved in the negative-bias temperature instability, IEEE Trans. Device Mat. Re. 7 (2007) 540–557.

[63] T. Su, Y. Yang, Y. Na, R. Fan, L. Li, L. Wei, B. Yang, W. Cao, An insight into the role of oxygen vacancy in hydrogenated $TiO_2$ nanocrystals in the performance of dye-sensitized solar cells, ACS Appl. Mater. Interfaces 7 (2015) 3754–3763.

[64] Z. Barbierikova, M. Bella, J. Kucerak, V. Milata, S. Jantova, D. Dvoranova, M. Vesela, A. Stasko, V. Brezova, Photoinduced superoxide radical anion and singlet oxygen generation in the presence of novel selenadiazoloquinolones (an EPR Study), Photochem. Photobio. 87 (2011) 32–44.

[65] K.C. Das, H.P. Misra, Hydroxyl radical scavenging and singlet oxygen quenching properties of polyamines, Mol. Cell. Biochem. 262 (2004) 127–133.

[66] C.E. Diaz-Uribe, M.C. Daza, F. Martínez, E.A. Páez-Mozo, C.L.B. Guedes, E. Di Mauro, Visible light superoxide radical anion generation by tetra(4-carboxyphenyl) porphyrin/$TiO_2$: EPR characterization, J. Photochem. Photobio. A-Chem. 215 (2010) 172–178.

[67] N. Zhou, T. Qiu, L.Y. Ping, L. Yang, Superoxide anion radical generation in the NaOH/$H_2O_2$/Fe(III) system: a spin trapping ESR study, Magn. Reson. Chem. 44 (2006) 38–44.

[68] N.A. Romero, D.A. Nicewicz, Organic photoredox catalysis, Chem. Rev. 116 (2016) 10075–10166.

[69] D. Ravelli, M. Fagnoni, A. Albini, Photoorganocatalysis. What for? Chem. Soc. Rev. 42 (2013) 97–113.

[70] D. Petzolda, B. Königa, Photocatalytic oxidative bromination of electron-rich arenes and heteroarenes by anthraquinone, Adv. Syn. Catal. 360 (2017) 626–630.

[71] W. Zhang, I.W.C.E. Arends, F. Hollmann, Selective photooxidation reactions using water-soluble anthraquinone photocatalysts, ChemCatChem 9 (2017) 3821–3826.

[72] S. Lerch, L.N. Unkel, M. Brasholz, Tandem organocatalysis and photocatalysis: an anthraquinone-catalyzed indole-C3-alkylation/photooxidation/1,2-shift sequence, Angew Chem. Int. Ed. Eng. 53 (2014) 6558–6562.

[73] R. Kavitha, S.G. Kumar, A review on plasmonic Au-ZnO heterojunction photocatalysts: preparation, modifications and related charge carrier dynamics, Mater. Sci. Semicond. Process. 93 (2019) 59–91.